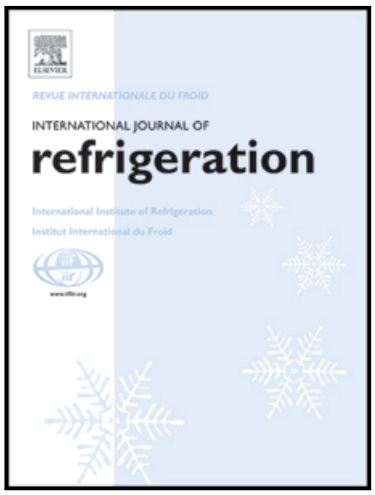

Design and optimization of regenerators of a rotary magnetic refrigeration device using a detailed simulation model

Behzad Monfared

PII: S0140-7007(18)30029-X
DOI: 10.1016/j.ijrefrig.2018.01.011
Reference: JIJR 3873

To appear in: *International Journal of Refrigeration*

Received date: 21 September 2017
Revised date: 7 January 2018
Accepted date: 14 January 2018

Please cite this article as: Behzad Monfared , Design and optimization of regenerators of a rotary magnetic refrigeration device using a detailed simulation model, *International Journal of Refrigeration* (2018), doi: 10.1016/j.ijrefrig.2018.01.011

Highlights

- 3D model of parasitic heat transfer is inserted in 1D model of active regeneration
- Validated model of magnetic refrigeration is used for optimization of regenerators
- High pressure drop can limit the benefits of giant magnetocaloric effect
- Effect of epoxy-binding refrigerant particles on the performance is investigated
- Thermal resistivity of epoxy cannot always be ignored despite its low mass

Design and optimization of regenerators of a rotary magnetic refrigeration device using a detailed simulation model

Behzad Monfared[a,*]

[a] KTH Royal Institute of Technology, School of Industrial Engineering and Management, Department of Energy Technology, Brinellvägen 68, SE-100 44 Stockholm, Sweden

* Corresponding author. Tel.: +46 8 790 81 54; fax.: +46 8 20 41 61.

E-mail address: behzadam@kth.se (Behzad Monfared)

Abstract

In this work a comprehensive simulation of a magnetic refrigeration device is presented, validated, and used for redesigning the regenerators of an existing prototype. The redesigning process includes choosing the magnetocaloric materials and number of layers and optimizing for particle size, flow, and operation frequency. The simulation consists of the model of the magnetic field, parasitic heat transfer and active regeneration. The model of the magnetic field and parasitic heat transfer are embedded in the 1D model of the active regeneration cycle. The detailed model of the magnetic field, taking the effect of presence of the magnetocaloric materials into account, is described and validated separately against measured magnetic field. An innovative method for including the parasitic heat transfer in the active regeneration model without compromising the accuracy is used. The influence of the properties of the binding agent on the performance of the bonded beds as regenerators are also investigated.

Keywords: Magnetic refrigeration, Modelling, Heat transfer, Regeneration, Bonded regenerator, Optimization.

Nomenclature:

a	specific surface area, ratio of heat transfer surface area of particles to volume of bed [m^{-1}]
A_c	cross section area of regenerator [m^2]
B	magnetic flux density [T]
COP	coefficient of performance
c_H	constant-field specific heat capacity [$Jkg^{-1}K^{-1}$]
c_p	constant-pressure specific heat capacity [$Jkg^{-1}K^{-1}$]
D_z	demagnetizing factor of the regenerators shape without porosity
d_P	diameter of particles [m]
H	magnetic field strength [Am^{-1}]
h	convection heat transfer coefficient [$Wm^{-2}K^{-1}$]
i	enthalpy [Jkg^{-1}]
k	thermal conductivity [$Wm^{-1}K^{-1}$]
M	magnetization [Am^{-1}]
$\dot{m}$	mass flow rate [kgs^{-1}]
m_r	mass ratio of epoxy to magnetocaloric material

N demagnetizing factor of a packed bed of particles

Nr number of regenerators

P pressure [Pa]

Pr Prandtl number [-]

p perimeter of cross section of regenerator [m]

$Q_{C,gross}$ gross cooling capacity including part of the parasitic heat transfer [W]

$Q_{C,net}$ useful cooling capacity [W]

Q_H heating capacity [W]

$Q_{par,c}$ parasitic heat transfer as concentrated load at cold end [W]

$q_{par,dist}$ distributed parasitic heat flux [Wm^{-2}]

$Q_{par,dist}$ rate of the total distributed parasitic load [W]

Re_d Reynolds number, $\rho_f.V_D.d_P/\mu_f$ [-]

s entropy [$Jkg^{-1}K^{-1}$]

T temperature [K]

$\bar{T}$ average temperature [K]

t time [s]

V volume [m^3]

V_D volumetric flow rate divided by cross section area of regenerator [ms^{-1}]

$\dot{W}$ mechanical power [W]

x position along regenerator [m]

Greek symbols

δ thickness [m]

ΔT_{Curie} Curie temperature minus average temperature of solid during a cycle (for each layer) [K]

ε porosity

ε_1 porosity in absence of epoxy

Λ_{cool} figure of merit, magnet design efficiency parameter

μ viscosity [Pas]

ρ density [kgm^{-3}]

τ cycle period [s]

Subscripts

amb ambient

bed packed bed of magnetocaloric materials

C cold reservoir

corr corrected

dist distributed

e epoxy

ef effective

ex external

f heat transfer fluid

H hot reservoir

in internal

L fluid leaving the regenerator

mag magnetic

R fluid returning from heat exchanger

s solid phase in regenerator

sf solid-fluid interface in regenerator

tot total

1 Introduction

Magnetic refrigeration at room temperature, as an alternative to the vapor-compression technology, has been the subject of many studies during the recent decades. The main motivation behind the research in this field is to avoid the use of ozone depleting or greenhouse gases as

working fluid and to reach higher energy efficiencies compared to vapor-compression technology.

The refrigerant in magnetic refrigeration, the magnetocaloric material, is usually a solid material which shows temperature increase when exposed in adiabatic condition to an external magnetic field. This magnetically induced change, called magnetocaloric effect, shows itself as reduction in entropy when magnetization is done in isothermal condition. The magnetocaloric effect is the strongest near the Curie temperature or magnetic phase transition temperature of the materials. By removing the heat from the magnetized material and subsequently demagnetizing it, the material becomes cold and can be used for refrigeration purposes. By making a rather long porous medium of magnetocaloric materials and blowing a heat transfer fluid in alternating directions (regeneration) synchronized with magnetization and demagnetization processes, the temperature difference between the two ends of the porous medium become greater than the magnetocaloric effect and can be large enough to make the magnetic refrigeration device suitable for actual applications. The cycle in which the magnetocaloric material is both refrigerant and regenerator is called active magnetic regeneration (AMR) cycle. In addition, by choosing materials with different transition temperatures matching the working temperatures as subsequent layers along the regenerator the temperature span or the cooling capacity can be increased further. Pecharsky and Gschneidner Jr (1999) have given more detailed explanations about the working principle of the magnetic refrigeration devices.

The most common magnetocaloric material used for room-temperature refrigeration is gadolinium (Gd), which goes through a second-order phase transition when magnetized (Romero Gómez et al., 2013). Because of the larger magnetic entropy change (magnetocaloric effect) in materials showing first-order phase transition, they are suggested for increasing the cooling capacity of room temperature magnetic refrigeration devices. $La(Fe,Mn,Si)_{13}H_z$ materials with tunable transition temperature are among the most promising materials going through first-order phase transition with adiabatic temperature change comparable with gadolinium, higher magnetic entropy change, almost unchanged magnetocaloric effect when their transition temperatures are altered via changing composition, very low hysteresis, and relatively high thermal conductivity compared to other magnetocaloric materials (Bahl et al., 2017; Morrison et al., 2012; Radulov et al., 2015).

A frequently mentioned drawback of materials with first-order phase transition, including $La(Fe,Mn,Si)_{13}H_z$, is the narrow peak of their magnetocaloric effect in the vicinity of the transition temperature, which makes them more sensitive to their working temperature. In addition, $La(Fe,Mn,Si)_{13}H_z$ is brittle and as a practical solution a binding agent such as epoxy is used to prevent them from pulverization. This extra layer of epoxy can hinder the heat transfer from the particles to the heat transfer fluid and also leaves narrower passages for the flow which increases the pressure drop. In addition, the magnetic properties are not uniform in each layer of these materials due to manufacturing difficulties; that is, there is a spread in the transition temperature of the materials manufactured with a nominal transition temperature (Monfared and

Palm, 2016; Neves Bez et al., 2016; Radulov et al., 2015). Considering these drawbacks, their superiority over the second-order phase transition materials such as gadolinium should be investigated.

The built prototypes are recently reviewed by Balli et al. (2017), who have categorized them by the employed magnetocaloric material and by Kitanovski et al. (2015), who have categorized them by their design. Among these prototypes, the prototype made by Astronautics delivering 2502 W cooling capacity over 11 K temperature span is remarkable among the magnetic refrigeration devices using permanent magnets due to its high cooling capacity. It uses a magnet assembly creating a rather large field of 1.44 T and operates with about 1.5 kg $La(Fe,Si)_{13}H_z$ alloys (Jacobs et al., 2014). Tura and Rowe (2011) have reported a rotary prototype with two sets of nested Halbach magnet assemblies with Λ_{cool} as defined by Bjørk et al. (2010) of 0.02 $T^{2/3}$. It is designed with emphasis on reducing the amount of magnetocaloric materials and increasing the operation frequency. Therefore, among the prototypes built so far, their prototype shows one of the highest exergetic cooling powers per unit magnetic field and unit volume of magnetocaloric material, 0.085 $WT^{-1}cm^{-3}$. A second-generation device based on this design is reported by Arnold et al. (2014) in which the magnet design is improved to create more desirable waveform during operation and allow for more optimum aspect ratio for the regenerators placed inside the magnet assemblies. Another notable prototype designed to operate at high frequency is presented by Engelbrecht et al. (2012). It has a rather complicated, rotary magnet assembly design with 0.0073 m^3 magnet and high figure of merit of Λ_{cool} = 0.2 $T^{2/3}$ and 24 stationary regenerators delivering 100 W cooling capacity over 20.5 K temperature span with 2.8 kg gadolinium as refrigerant. Among the reciprocating designs the prototype presented by Balli et al. (2012) and Sari and Balli (2014) can be mentioned with two parallel magnet assemblies creating 1.45 T field, initially designed to deliver 80 to 100 W cooling capacity over 20 K temperature span. The maximum temperature span of 30 K created by this device is one of the largest temperature spans created by devices using permanent magnets.

We also have a prototype in the Department of Energy Technology, KTH Royal Institute of Technology, Stockholm, introduced first by Monfared and Palm (2016). This prototype is initially designed to replace a vapor-compression system of a professional refrigerator with small amount of permanent magnet material used. The magnetic circuit design[1] is inspired by the work of Okamura et al. (2007). The figure of merit Λ_{cool}, showing how efficiently the 0.00045 m^3 magnet material is used, is 0.2 $T^{2/3}$ for this magnetic circuit. This value is close to the best value in the review article by Bjørk et al. (2010) and a similar design with larger amount of magnet, 0.0019 m^3, reported by Lozano et al. (2016). However, due to problems such as corrosion, pulverization of the magnetocaloric materials, and clogging of the flow passages of the regenerators, running systematic tests was challenging. In addition, in the initial design some details were ignored. Therefore, redesigning the regenerators was necessary.

[1] The magnetic circuit is not designed by the author.

The tool used for redesigning the regenerators is a simulation computer model. It consists of three parts: a model of the external and internal magnetic field, a model of the parasitic heat transfer, and a model of the active magnetic regeneration cycle. For modeling the magnetic field the effect of presence of the magnetocaloric materials on the external field is considered. The parasitic heat transfer is added as an innovative phenomenological model relating the actual complex, three-dimensional heat transfer to a simple one-dimensional model, which is easily inserted in the active magnetic regeneration cycle model. In the model of active magnetic regeneration cycle the conductive resistance inside the particles is considered and equations to include the effect of adding a binding agent to the packed bed of particles are derived. The whole model is explained in detail in section 3 of this article.

The simulation model is validated against experimental results obtained from the prototype filled with gadolinium (Gd). Then, using the validated model, the necessity of layering the regenerator with different materials and the benefits of using magnetocaloric materials with first order phase transition, such as $La(Fe,Mn,Si)_{13}H_z$, are investigated. The regenerators are also redesigned and optimized to fit the working conditions of a refrigerator. In addition, the results are discussed and conclusions are drawn.

2 Prototype

The prototype modeled in this work and used for validation is of rotary type with rotating magnet assembly and fixed regenerators. The regenerators are packed beds of magnetocaloric particles. As shown in Figure 1, the prototype is designed with 12 regenerators. However, with minor adjustments, the prototype can be run with only 2, 4, or 6 regenerators, as well. The volume of each regenerator is 31.2±0.1 cm^3 and the length is 15 cm. Two headers cover the ends of the regenerators with separate inlets and outlets for the heat transfer fluid.

Figure 1: The regenerators' casing filled with magentocaloric materials

The magnetic field is created by an assembly consisting of pieces of permanent magnets with rectangular cross section, shown by dark grey in Figure 2, and soft magnetic materials, shown by light grey. The magnet assembly creates two high field regions, at positions 12 and 6 o'clock in Figure 2, and two low field regions, at positions 3 and 9 o'clock (see Figure 8 for the magnetic

field inside a regenerator at each angular position of the magnet assembly when all the regenerators are empty). Rotation of the magnet assembly changes the external field experienced by the regenerators, as depicted in Figure 3. Thus, the regenerators at two ends of the casing's diameters go through similar cycles. To concentrate the field and guide the field lines, the casing of the regenerators is placed inside a laminated yoke (the light grey cylinder in Figure 2). The lamination is to prevent eddy electric currents caused by the changing magnetic field as the magnet assembly rotates.

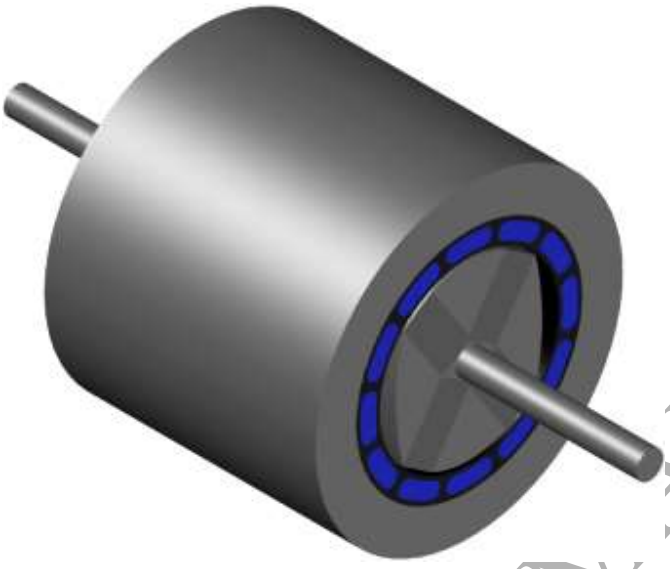

Figure 2: The magnet assembly, the regenerators, and the yoke

As the magnet rotates, the magnetized regenerators (marked red in Figure 3) remain in the high field region during about 30° rotation angle. While the regenerators are in high field region, the heat transfer fluid flows from the cold end to the warm end. As the magnet continues its rotation the flow goes through the next regenerators; therefore, the warm fluid leaving the regenerators and entering the warm heat exchanger is unidirectional, allowing the heat exchanger to operate efficiently. The flow in the opposite direction for the demagnetized regenerators (marked blue in Figure 3) and in the cold heat exchanger is similar. For distributing the heat transfer fluid between the regenerators a rotary valve, coupled mechanically to the magnet shaft, is used. The rotary valve is synchronized with the magnet assembly in the way that the heat transfer fluid flows through a regenerator only while it is in the maximum or minimum magnetic field region, which corresponds to about 30° rotation of the magnet assembly. For laboratory tests the magnet assembly is rotated by a stepper motor to have full control over the magnet position, including rotating continuously at different, constant speeds, e.g. Figure 16b, or intermittent rotation, e.g. Figure 12b.

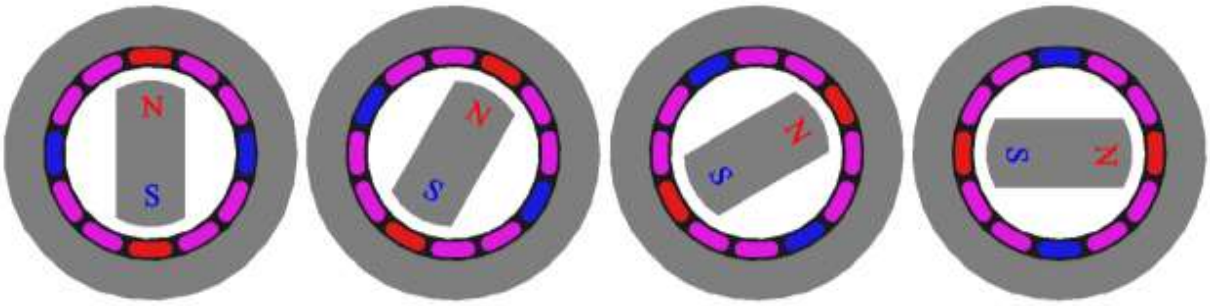

Figure 3: Magnetized regenerators (red) and demagnetized regenerators (blue) during 90° rotation of magnet assembly with maximum number of regenerators used

For the experimental tests reported in this article, the cold heat exchanger is replaced by an electric heater to have better control over the cooling load. The warm heat exchanger is an air cooled heat exchanger with a fan and the whole prototype including the heat source and the warm heat exchanger is placed in a climate chamber to have control over the ambient temperature.

Apart from the heat transfer mechanisms within the regenerators, which are covered in section 3.3 where the modeled active magnetic regeneration cycle is described, some parasitic heat is transferred from the surroundings to the regenerators and the electrical heater and also from the warm end of the regenerators through the nearby solid materials, including the casing of the regenerators, the yoke, and the magnet assembly, to the cold end. To reduce the parasitic heat transfer a 1 mm air gap is created between the regenerators' casing and the yoke and insulating materials are placed over the yoke, header of the regenerators' casing on the cold end, and the electrical heater and its connecting tubes.

3 Modeling

The simulation model consists of three parts: a model of the external and internal magnetic field, a model of the parasitic heat transfer, and a model of the active magnetic regeneration cycle.

By the model of the magnetic field, the homogeneity of the external magnetic field is investigated, the model is validated against measured values, and the internal field is calculated taking demagnetizing effect into account.

For the parasitic heat transfer, a three-dimensional model is created and its results are used to derive a one-dimensional model, convenient to use together with the model of the active magnetic regeneration cycle.

The active magnetic regeneration cycle is modeled as a one-dimensional, transient model, in which the results of the two other parts of the model are used.

3.1 Magnetic field

The whole magnetic circuit, shown in Figure 2, is modeled in 3D in COMSOL. In the model, when applicable, presence of the magnetocaloric materials in the space between the magnet assembly and the yoke is taken into account to model the magnetic field more accurately. It is done by defining a field dependent equivalent permeability for the regenerators, which corresponds to the average permeability of the void space and the magnetocaloric material weighted by their volume. Figure 4 shows the direction and strength of the magnetic field in a cross section of a setup with regenerators filled with $La(Fe,Mn,Si)_{13}H_z$ particles at their transition temperature.

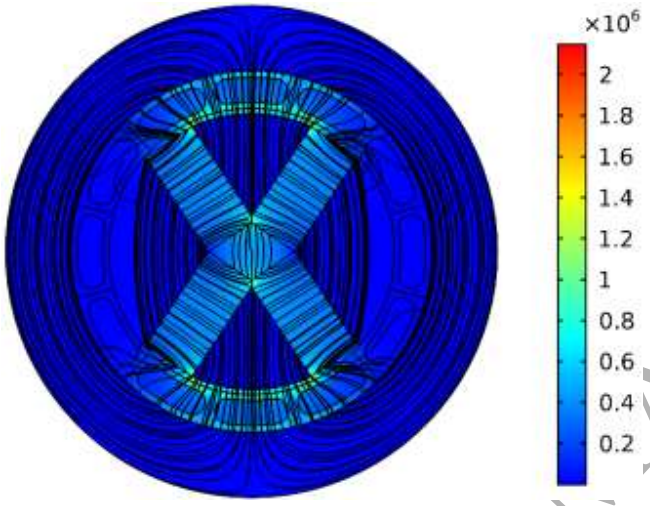

Figure 4: The magnetic field strength [Am^{-1}] when all regenerators are filled (the density of the lines is not proportional to the field strength)

3.1.1 Uniformity of the magnetic field

To simplify the model, it is advantageous to have a single value for the magnetic field inside the whole regenerator at each time step when working with the differential equation Eq. 2 introduced in section 3.3. To examine the validity of this assumption, the magnetic fields along three arbitrary lines, shown in Figure 5, are evaluated at different rotation angles of the magnet assembly. The results, which are analyzed further, for six rotation angles are presented in Figure 6. For investigating the uniformity of the field it is assumed that the regenerators are filled with $La(Fe,Mn,Si)_{13}H_z$ particles.

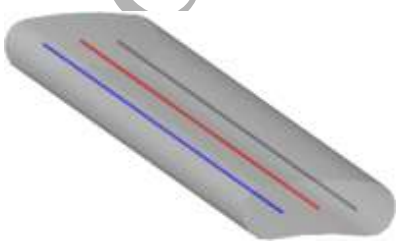

Figure 5: Arbitrary lines along which the magnetic field is evaluated

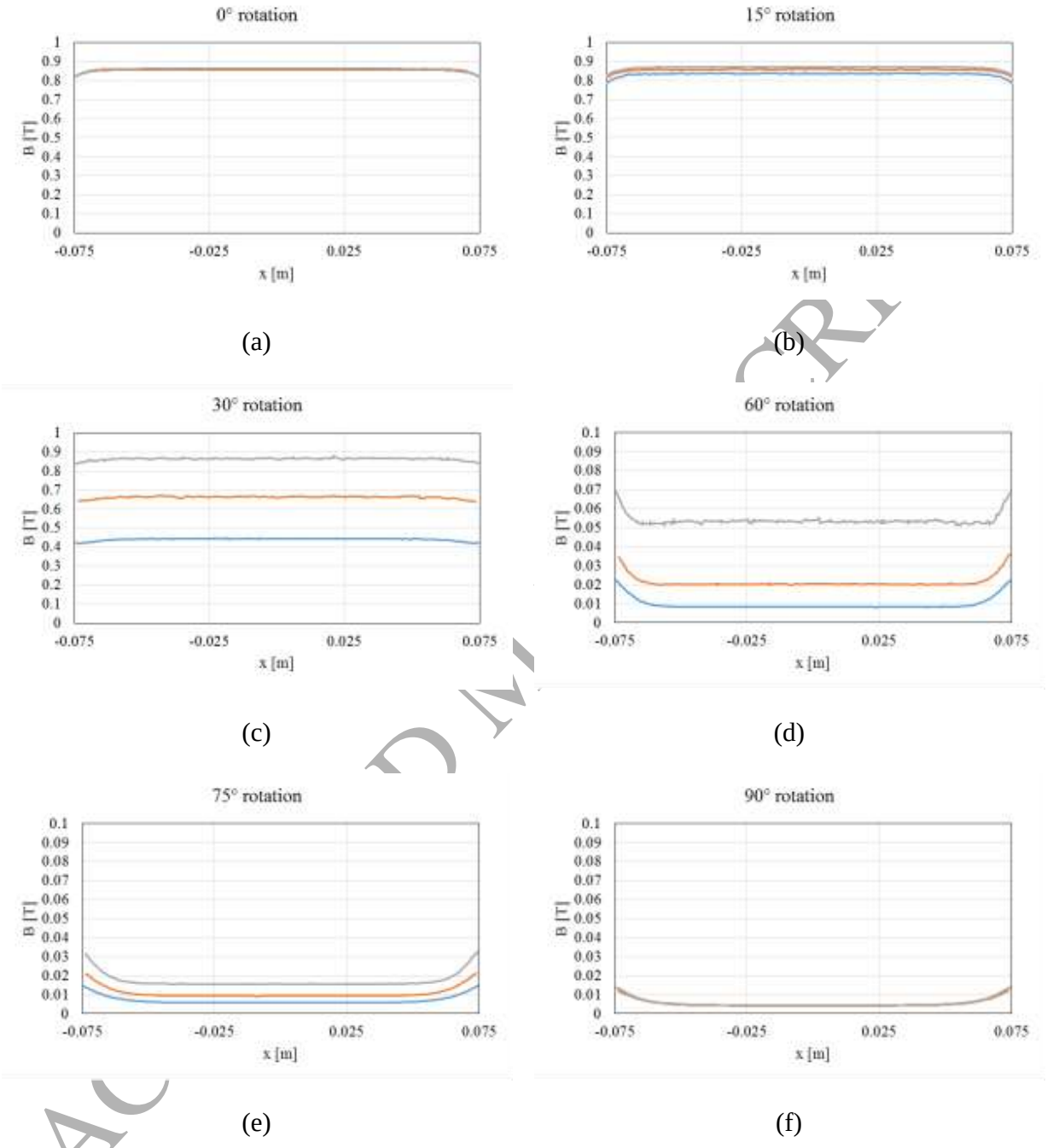

Figure 6: Magnetic field along the three lines shown in Figure 5 for the following rotation angles of the magnet assembly: (a) 0°, (b)15°, (c) 30°, (d) 60°, (e) 75°, and (f) 90°

In Figure 6a, the field is maximum in the entire regenerator and remains high while the magnet is at a range ±15° about this position (Figure 6b). Within this 30° range the field on different lines

are virtually the same, showing the uniformity of the field in azimuthal direction. At the two ends the lines are bent slightly downwards showing the end effects; however, the field close to the two ends is not significantly different from the field at inner positions. Figure 6c shows that when the magnet assembly has rotated further and the regenerator has left the high field region, the field is different on the three lines although it is quite uniform along each of them in axial direction. Such differences in azimuthal direction is expected since as the magnet rotates, some parts of the regenerator may still be in the high field region or close to it while the rest of it has left the high field region. When the magnet assembly is at such intermediate positions on its way to rotate further until the regenerator enters low field region completely, the only ongoing processes are a weak heat transfer between the solid material and the stationary fluid and weak heat transfer through conduction. For that reason, by doing calculations based on the average of the magnetic field in azimuthal direction no significant phenomenon is missed. Figure 6d is similar to Figure 6c, but the difference between the fields on different lines are much smaller (notice the change of the scale of the vertical axis). In Figure 6d the end effect is magnified due to the choice of scale of the plot. Still there is no flow through the regenerator before the magnet assembly rotates 75°. Figure 6e and Figure 6f show that when the regenerator is in the low field region (a nearly ±15° range about 90° rotation angle), the variation in the azimuthal direction disappears again. The end effects, although magnified in this plot due to the choice of the scale, is negligible and the field is in practice zero through entire regenerator.

In conclusion, a single value for the magnetic field inside the whole regenerator at each time step can be used in the model of the active magnetic regeneration cycle explained in section 3.3.

3.1.2 Validation of the magnetic field model

The model created for the magnetic field is validated using two series of measured values. For the measured values shown in Figure 7 two regenerators making a right angle were filled with gadolinium and the probe was placed in the plastic casing outside one of the filled regenerators at the depth of 34 mm from the edge of the yoke and at 12° angle relative to the center of the adjacent, filled regenerator. The measurements are done using Electromagnetic Field Meter PCE-MFM 3000, with accuracy of ± (5% of reading + 0.001 T). As can be seen in Figure 7, neglecting the magnetocaloric materials in the magnetic field model can result in values which are not within the accuracy range of the measured ones when the field is high, while taking the effect of filled regenerators into account produces results matching the measured one.

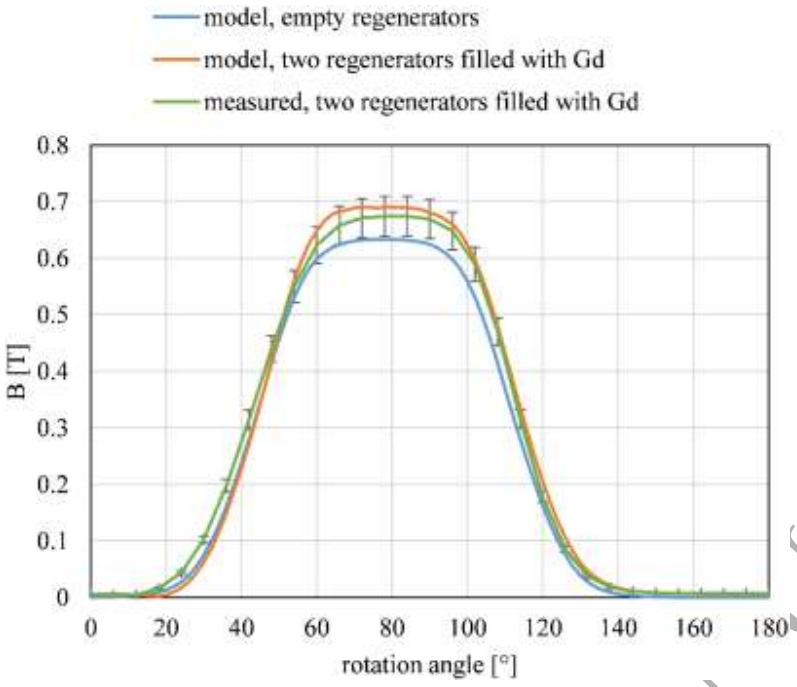

Figure 7: Modeled magnetic field compared to the measured field at a certain point with two regenerators filled with Gd. The bars show the accuracy of the measurement instrument.

The second series of the measurements shown in Figure 8 were done with an instrument with higher precision at 16 different axial positions along an empty regenerator and different rotation angles of the magnet assembly. The instrument used is a SENIS 3-Axis magnetic field transducer, and the field sensitive volume of its 3D Hall sensor is $0.15 \times 0.01 \times 0.15$ mm^3. The measured values are accurate within a ±1% range. For these measurements all of the regenerators were empty. As Figure 8 shows, the model matches the measured values well when the field is maximum and minimum, which are the most important values for simulating the active magnetic regeneration cycle. The discrepancies at the transition between maximum and minimum field can be related to the position of the small probe used, measuring the local field: as explained earlier at the transient rotation angles the field is not uniform in azimuthal direction and position of the probe has an influence on the readings.

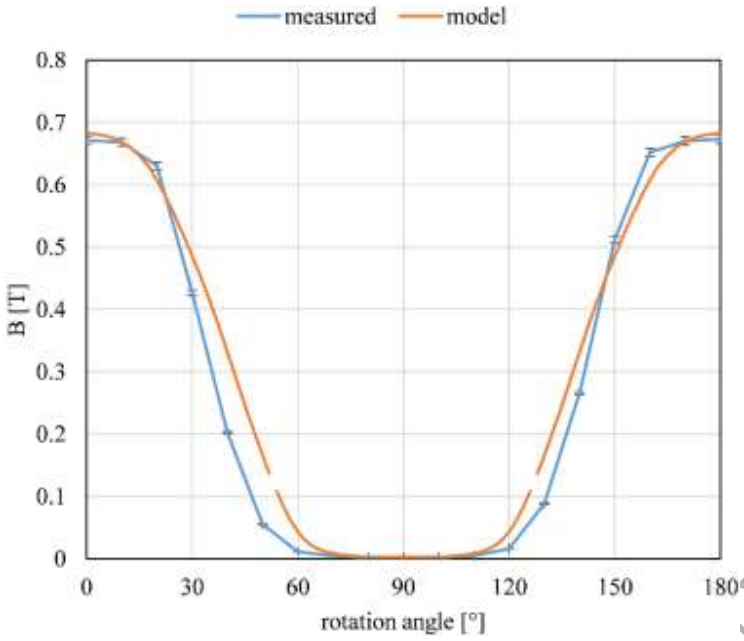

Figure 8: Measured and modeled magnetic field with empty regenerators. The bars show the accuracy of the measurement instrument.

3.1.3 Differentiating between internal and external magnetic field

Due to demagnetizing effect the magnetic field inside a magnetized material is different from the external magnetic field to which it is exposed (Morrish, 2001). Bleaney and Hull (1941) suggest that for a packed bed of ellipsoidal particles the internal magnetic field can be related to the external field using Eq. 1 with demagnetizing factor given by Eq. 2. Bjørk and Bahl (2013) have further investigated the applicability of Eq. 2 to the packed bed regenerators in room temperature magnetic refrigeration devices and confirmed its validity for materials with relative permeability close to that of magnetocaloric materials such as gadolinium and $La(Fe,Mn,Si)_{13}H_z$ in vicinity of their magnetic transition temperatures and external field of 1T.

$$H_{in} = H_{ex} - NM \tag{1}$$

$$N = \frac{1}{3} + (1 - \varepsilon)\left(D_z - \frac{1}{3}\right) \tag{2}$$

Differentiating between internal and external magnetic field is important as the field-dependent properties of the magnetocaloric materials vary with the internal field, not the external. Therefore, the measured properties of the materials used in the simulations in this work, in case they are reported for different external fields and temperatures in their source, are first related to the internal field by using the demagnetizing factor of the measurement sample. Then, in the model simulating active magnetic regeneration cycle the external field created by the magnet assembly is converted to the internal field (using Eq. 1 and Eq. 2) to evaluate the properties of the magnetocaloric materials at each time step. In other words, the output of the modeled magnetic

field described in this section is the external field, which is later converted into internal field in the simulation model of the active magnetic regeneration cycle explained in section 3.3.

3.2 Parasitic heat transfer

To investigate the rate of parasitic heat transfer mentioned in section 2, a three-dimensional, steady state model is created in COMSOL. The geometry used in this model is shown in Figure 9. The essential parts of the heat transfer model not visible in Figure 9 are: the 1 mm air gap between the regenerators' casing and the yoke; the electrical heater and its connecting tubes; and insulating material. An assumption made in the model is that the temperature within the regenerator varies linearly from the cold end to the warm end. A simplification made to avoid complicated transient modeling is that the non-cylindrical magnet assembly, which has different angular positions during operation of the prototype, is modeled as a cylinder with the size of the volume swept by the magnet assembly and average thermal properties of permanent magnet material, soft magnetic material, and air weighted by their mass.

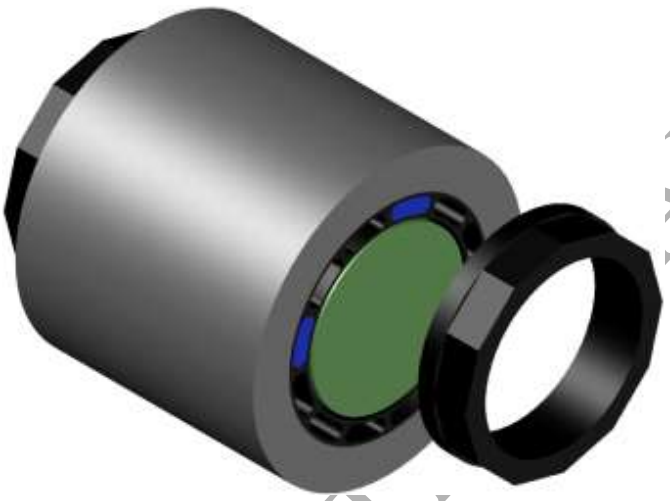

Figure 9: Heat transfer model for a case with two regenerators in use (the insulating materials, heater and connecting hoses are not shown for clarity of the figure). One of the headers is removed to show the inside of the regenerators' casing.

Although the heat transfer model is rather complicated and is three dimensional, a phenomenological model, suitable for implementing in the one dimensional model of the active magnetic regeneration cycle, is derived based on it.

After running the heat transfer model for the temperatures obtained from the experimental tests reported in section 4, it is observed that the heat flux to a regenerator at each axial position, apart from nearly 1 cm at the cold end and few millimeters at the warm end, is a linear function of the temperature difference between the ambient and the regenerator at that point. Figure 10 shows the heat flux to the regenerator for one of the experimental tests reported in section 4 (with 6 W cooling load) and a hypothetical case with 30 K temperature difference between the cold and warm ends and ambient temperature 2 K lower than the warm end, showing that the phenomenological model works well for larger temperature spans as well. The slopes of the

linear parts of the investigated tests are close and an average value of them can be used; the intercept itself is a linear function of the temperature difference between the warm and cold ends. The nonlinear part of the heat flux to the cold end, the magnitude of which depends on the cold end temperature, is integrated and estimated as a concentrated load at the cold end. The magnitude of this concentrated load is proportional to the temperature difference between the ambient and the cold end. The nonlinear part at the warm end is neglected.

Another part of the parasitic load is the transferred heat from the ambient to the electrical heater and its connecting tubes. This load is modeled as a linear function of the temperature difference between ambient and the average cold end temperature of the heat transfer fluid.

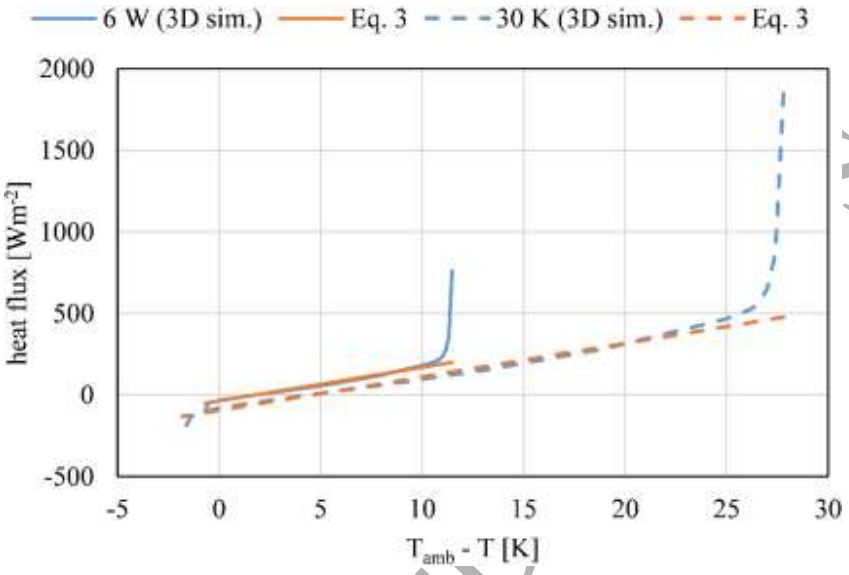

Figure 10: Calculated parasitic heat flux to a regenerator for the test with 6 W total cooling load reported in section 4 and a case with 30 K temperature difference between cold and warm ends. Eq. 3 gives the linear approximation of the middle part.

In brief, the parasitic heat transfer for the tests used for validation of the model in section 4 is implemented in the model of the active magnetic regeneration cycle as Eq. 3 (the distributed load as local heat flux through the boundary between a regenerator and its casing) and Eq. 4 (concentrated load).

$$q_{par,dist} = 20.55\left(T_{amb} - T_f(x,t)\right) - \left(3.29\left(\bar{T}_{warm\ end,f} - \bar{T}_{cold\ end,f}\right) - 3.64\right) \quad (3)$$

$$Q_{par,c} = 0.0093\left(T_{amb} - \bar{T}_{cold\ end,f}\right) + 0.0646\left(T_{amb} - \bar{T}_{cold\ end,f}\right) \quad (4)$$

The first term on the right hand side of Eq. 4 corresponds to the integrated flux to the cold end and the second term corresponds to the heat transfer from the ambient to the electrical heater and its connecting tubes. In section 3.3 it is explained how these two equations are used in the model of the active magnetic regeneration cycle.

The combined radiative and convective heat transfer coefficient at the outer surface, which is used in the three dimensional model of heat transfer, is roughly estimated to 20 $Wm^{-2}K^{-1}$. This value is not certain due to the rather complicated geometry of the prototype and unknown direction and magnitude of air velocity at different places over the prototype while the tests were running. To investigate the effect of the uncertainty of this value a sensitivity analysis is done with convective heat transfer coefficients ranging from 10 to 40 $Wm^{-2}K^{-1}$ (corresponding to air velocity of about 15 ms^{-1}). The sensitivity analysis showed that the results do not change considerably (maximum 0.4 W in cooling capacity and 1 K in temperature span) with this parameter.

3.3 The active magnetic regeneration cycle

The active magnetic regeneration cycle is modeled using Eq. 5 and Eq. 6. Since the regenerators go through similar cycles, only one of them needs to be modeled and the calculated capacities and work rates can be multiplied by the number of the regenerators. Apart from the first term in Eq. 6, this is the system of partial differential equations suggested by Engelbrecht (2008) and used extensively by other researchers. The system of equations is solved numerically through iteration using Backward Time, Centered Space scheme to reach cyclic steady state. In the numerical solution both refrigerant and heat transfer fluid are initially at ambient temperature and the boundary conditions are given in Table 1. The number of time steps for each iteration is 8000. The spatial segments used for the numerical calculations is 16 cells for single-layer regenerators and six cells per layer for layered regenerators. Higher number of segments or time steps do not change the results.

$$-(1-\varepsilon)\rho_s T_s \frac{\partial s}{\partial B}\frac{\partial B}{\partial t} = -k_{ef,s}\frac{\partial^2 T_s}{\partial x^2} - h_{sf,corr}a\left(T_f - T_s\right) + (1-\varepsilon)\rho_s c_{H,s}\frac{\partial T_s}{\partial t} \quad (5)$$

$$\frac{p.q_{par,dist}}{A_c} + \frac{dP}{dx}V_D = \rho_f V_D c_{p,f}\frac{\partial T_f}{\partial x} - k_{ef,f}\frac{\partial^2 T_f}{\partial x^2} + h_{sf,corr}a\left(T_f - T_s\right) + \varepsilon\rho_f c_{p,f}\frac{\partial T_f}{\partial t} \quad (6)$$

Table 1: Boundary conditions

	Flow from cold end to warm end	Flow from warm end to cold end
Fluid, cold end	$T_f=T_{C,R}$	$\partial T_f/\partial x=0$
Fluid, warm end	$\partial T_f/\partial x=0$	$T_f=T_{H,R}$
Solid, cold/warm end	$\partial T_s/\partial x=0$	$\partial T_s/\partial x=0$

The first term in Eq. 6, which is not a constant but varies with T_f according to Eq.3, covers a part of the parasitic heat transfer explained in more detail in section 3.2. The correlations used for evaluating the effective thermal conductivities, $k_{ef,f}$ and $k_{ef,s}$, are Eq. 7 and Eq. 8 (Amiri and Vafai,

1998). The convection heat transfer coefficient, h_{sf}, is calculated using Eq. 9 (Wakao and Kaguei, 1982). The pressure drop, *dP/dx*, is calculated by modified Ergun equation, Eq. 10, (Macdonald et al., 1979). To take into account the conduction thermal resistance in the solid particles, h_{sf} is corrected according to Eq. 11 (Dixon and Cresswell, 1979; Nield and Bejan, 2013) for spherical particles.

$$k_{ef,f} = k_f(\varepsilon + 0.5Re_dPr) \quad (7)$$

$$k_{ef,s} = (1-\varepsilon)k_s \quad (8)$$

$$h_{sf} = \frac{k_f}{d_P}\left(2 + 1.1Pr^{1/3}Re_d^{0.6}\right) \quad (9)$$

$$-\frac{dP}{dx} = \frac{180(1-\varepsilon)^2\mu_f}{d_p^2\varepsilon^3}V_D + \frac{1.8\rho_f(1-\varepsilon)}{d_p\varepsilon^3}V_D^2 \quad (10)$$

$$\frac{1}{h_{sf,corr}} = \frac{1}{h_{sf}} + \frac{d_P}{10k_s} \quad (11)$$

Regarding the small diffusivity of the regenerators' casing material, 0.16 mm^2s^{-1}, and small ratio of thermal mass of the regenerators' walls to that of the magnetocaloric materials, about 0.2, the effect of walls acting as passive regenerators is negligible for the investigated working conditions (Nielsen et al., 2013). However, the role of the walls in increasing the conduction from the warm end to the cold end is included in the model of the parasitic heat transfer.

The properties of gadolinium used in the model are presented by Lozano et al. (2014). The properties of $La(Fe,Mn,Si)_{13}H_z$, except density and thermal conductivity, are published by Morrison et al. (2012). To model the gadolinium alloys and $La(Fe,Mn,Si)_{13}H_z$ with different transition temperatures, the temperature dependent properties of gadolinium and $LaFe_{11.384}Mn_{0.356}Si_{1.26}H_{1.52}$ are shifted and adjusted as explained by Monfared and Palm (2015), not to violate thermodynamic relations. Density of $La(Fe,Mn,Si)_{13}H_z$, 7100 kgm^{-3}, is given by Radulov et al. (2015). The measured thermal conductivity of similar materials, which varies between 8 and 8.8 $Wm^{-1}K^{-1}$ for the temperature range of interest in this work, are presented in the works by Fujieda et al. (2004) and Fukamichi et al. (2006). However, in this work the conservative, constant value of 8 $Wm^{-1}K^{-1}$ is used for the entire range. In the model, the properties, apart from density, of the heat transfer fluid, either aqueous solution of ethylene glycol or water, are temperature dependent and the effect of corrosion inhibitors on the properties is neglected (Melinder, 2010).

In all of the simulations the return temperature from the warm heat exchanger is an input to the model. When the cyclic steady state is reached, the heating capacity is calculated using Eq. 12.

$$Q_H = Nr\left(\int_{V_D>0} \dot{m}_f\, i_{H,L}\, dt - \int_{V_D<0} \dot{m}_f\, i_{H,R}\, dt\right)/\tau \quad (12)$$

In Eq. 12, $i_{H,L}$ and $i_{H,R}$ are the enthalpies of the heat transfer fluid leaving and entering (return from the warm heat exchanger) the warm end of the regenerator, respectively.

In case the return temperature from the cold heat exchanger is an input to the model, the gross cooling capacity (including part of the parasitic heat transfer) is calculated using Eq. 13.

$$Q_{C,gross} = Nr\left(\int_{V_D>0} \dot{m}_f \, i_{C,R}\, dt - \int_{V_D<0} \dot{m}_f \, i_{C,L}\, dt\right)/\tau \tag{13}$$

In Eq. 13, $i_{C,L}$ and $i_{C,R}$ are the enthalpies of the heat transfer fluid leaving and entering (return from the cold heat exchanger) the cold end of the regenerator, respectively.

The net (useful) cooling capacity is related to the gross cooling capacity according to Eq. 14.

$$Q_{C,net} = Q_{C,gross} - Q_{par,c} \tag{14}$$

In case the net cooling capacity is an input to the model, the enthalpy of the heat transfer liquid coming back from the cold source is calculated using Eq. 14 and Eq. 15. The temperature corresponding to this enthalpy is the temperature of heat transfer fluid entering the cold end, $T_{C,R}$.

$$i_{C,R} = \frac{\int_{V_D<0} \dot{m}_f \, i_{C,L}\, dt + Q_{C,gross}\,\tau}{\int_{V_D>0} \dot{m}_f\, dt} \tag{15}$$

The pumping power is calculated using Eq. 16.

$$\dot{W}_{pump} = Nr\left(\int_0^L \int_0^\tau |V_D| A_c \frac{dP}{dx} dt dx\right)/\tau \tag{16}$$

The rate of the total distributed parasitic load is given by Eq. 17.

$$Q_{par,dist} = Nr\left(\int_0^L \int_0^\tau pq_{par,dist}\, dt dx\right)/\tau \tag{17}$$

By an energy balance over the regenerator during the whole cycle the magnetic power can be deduced according to Eq. 18.

$$\dot{W}_{mag} = Q_H - Q_{C,gross} - \dot{W}_{pump} - Q_{par,dist} \tag{18}$$

3.3.1 Effect of binding agent

In case epoxy is used as a binding agent for keeping the particles at their place and increasing their mechanical strength, the corrected heat transfer coefficient is calculated using Eq. 19. The last term in this equation takes the thermal resistance of the epoxy, assuming a uniform layer of epoxy covering the whole heat transfer surface area, into account. The thickness of this layer can

be obtained from Eq. 20 when the mass ratio of epoxy to the magnetocaloric material is known. The mass ration of epoxy usually corresponds to the smallest amount of epoxy giving the desired mechanical strength (Neves Bez et al., 2016).

$$\frac{1}{h_{sf,corr}} = \frac{1}{h_{sf}} + \frac{d_P}{10k_s} + \frac{\delta_e}{k_e} \tag{19}$$

$$\delta_e = \frac{V_e}{a.V_{bed,tot}} = m_r.\frac{\rho_s}{\rho_e}\frac{d_p}{6} \tag{20}$$

The effective axial thermal conduction through the solid phase is influenced by the presence of epoxy and is corrected by adding conductivity of epoxy weighted by the volume it occupies (Eq. 21). The volume of epoxy also reduces the porosity, which in turn increases the pressure drop.

$$k_{ef,s} = k_s(1-\varepsilon_1) + k_e\frac{V_e}{V_{bed,tot}} = k_s(1-\varepsilon_1) + k_e(\varepsilon_1 - \varepsilon) \tag{21}$$

A total equivalent heat capacity can also be calculated for the solid phase; however, since the mass ratio of epoxy to the magnetocaloric material is very small, typically 2—3%, it does not affect the results significantly. In contrast, because of the relatively low density of the cured epoxy, the effects related to its volume are more significant and are taken into consideration in the model as explained in this subsection. In this work, the mass ratio of epoxy is 3%, the density of epoxy is 2090 kgm^{-3}, and two values of 1.16 $Wm^{-1}K^{-1}$ and 0.19 $Wm^{-1}K^{-1}$ are used for its thermal conductivity.

4 Validation

The experimental results, used for validation of the simulation model, are obtained with two regenerators filled with gadolinium with average particle diameter of 550 µm (standard deviation 55 µm) based on measuring 20 randomly selected particles (see Figure 11) and porosity of 0.36 at the following test conditions: ambient temperature of 21.6—22.1 °C; return temperature from warm heat exchanger of 22.4—22.7 °C; zero cooling load unless otherwise stated; 0.5 Hz cycle frequency unless the frequency variation is tested, maximum flow rate of 5.8 cm^3s^{-1} unless flow variation is tested; magnetic field and flow rate variation for each regenerator as indicated in Figure 12.

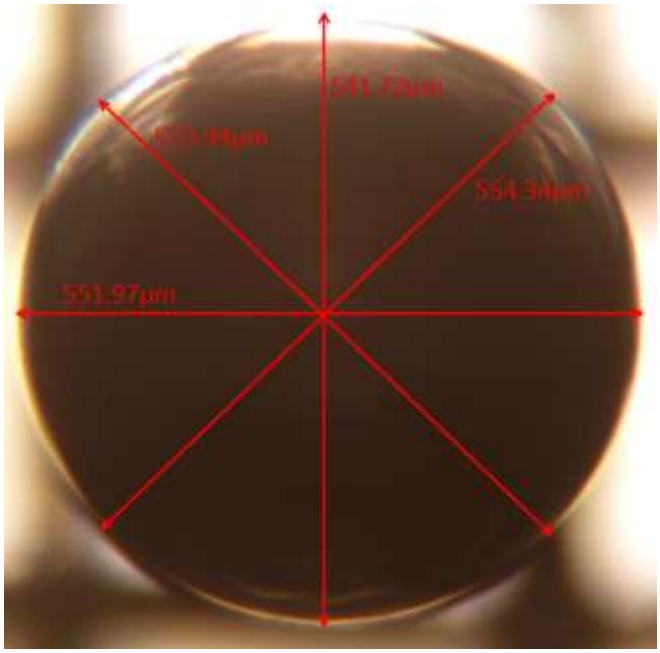

Figure 11: One of the randomly measured particles (the estimated sphericity is about 99.99%)

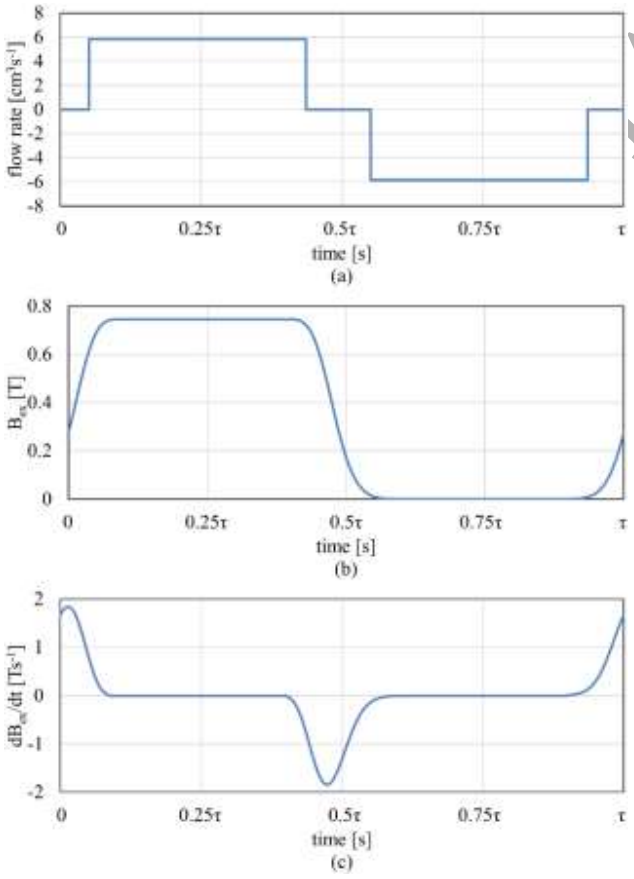

Figure 12: For the case with two regenerators filled with Gd: (a) flow in each regenerator (the maximum rates can be different in the tests) (b) external field (c) rate of change of the external field

The two regenerators filled with gadolinium make a right angle; that is, there are two empty regenerator spaces in between them. Since only two regenerators are used, it is possible to make the transition between the high field period and low field periods short and keep the magnet assembly stationary in the positions where it creates maximum or minimum field (compare the shape of Figure 12b with Figure 8). Accordingly, the periods during which the heat transfer fluid flows are extended, which allows to have the heat transferred from the particles with lower flow rate of the heat transfer fluid, and therefore, lower pressure drop. In addition, by keeping the period of transition between low and high magnetic field short, less time is available to unwanted phenomena such as axial conduction from warm end to cold end through the regenerators and outside regenerators and the parasitic heat transfer from the ambient to the regenerators.

In the experimental tests, the heat transfer fluid is a 15% by volume aqueous solution of ethylene glycol containing corrosion inhibitors.

The temperature span is defined as the difference between the temperature of the heat transfer fluid returning from the warm heat exchanger and returning from the cold source (electrical heater). Figure 13 shows the results of experimental tests and simulations for different cycle frequencies. The simulated values are very close to the measured ones.

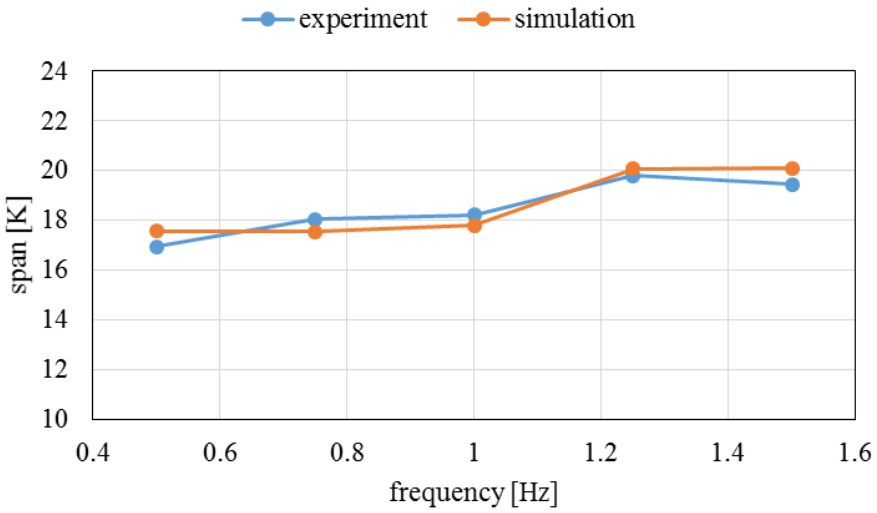

Figure 13: Tests with varied cycle frequency with two regenerators filled with gadolinium

The results of the tests in which the maximum flow rate is varied are presented in Figure 14. For the case with 4.1 W total cooling load the experimental and simulation results are very close. For the tests with no cooling load, the largest difference between the simulated results and the measured ones is less than 2 K. The difference at the flow rate giving the maximum temperature span for the no-load tests is about 1 K; it is less for lower flow rates.

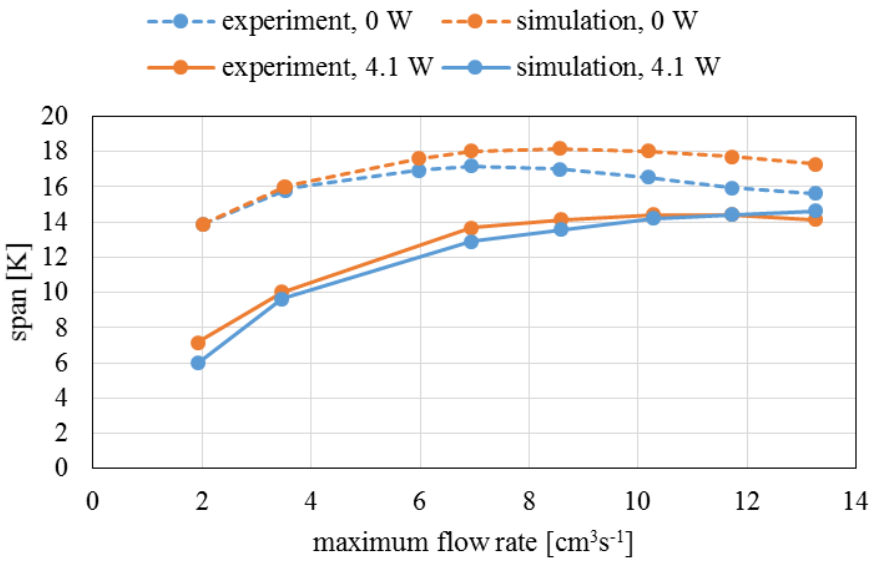

Figure 14: Tests with varied flow rate of heat transfer fluid with two regenerators filled with gadolinium and total cooling loads of 0 and 4.1 W

In Figure 15 the simulated results and the measured ones are compared for different cooling loads. For temperature spans larger than 10 K there is a good agreement between the simulated and measured results. However, with smaller temperature spans, which are also less interesting from the application point of view, the simulation under predict the performance of the prototype. In these tests the cooling capacity is given as input to the simulation model. The input cooling capacity affects the enthalpy of the heat transfer fluid coming back from the cold heat exchanger through Eq. 14 and Eq. 15, and thereby, it affects the temperature at the colder end of the regenerator. Although the cooling capacity determines the temperature at the cold end, it is not directly related to any loss mechanism, whereas the temperatures along the bed and at the two ends are directly related to loss mechanisms such as parasitic heat transfer from the ambient and axial heat transfer. Therefore, such temperature dependent loss mechanisms are investigated thoroughly and their parameters are modified to see whether the physical models from which they are derived are inaccurate. Nevertheless, these attempts did not reveal how the difference between the experimental results and the simulation results for high cold end temperatures (very small spans) can be corrected for. It should also be noted that the span is defined as the temperature difference between the heat transfer fluids coming back from the warm heat exchanger and the electrical heater; that is, within the range where the simulation over predict the performance, in a device with approach temperature difference of, say, 3 K in the warm and cold heat exchangers, the difference between the heat sink and heat source would be 4 K and below, which has no or limited practical use.

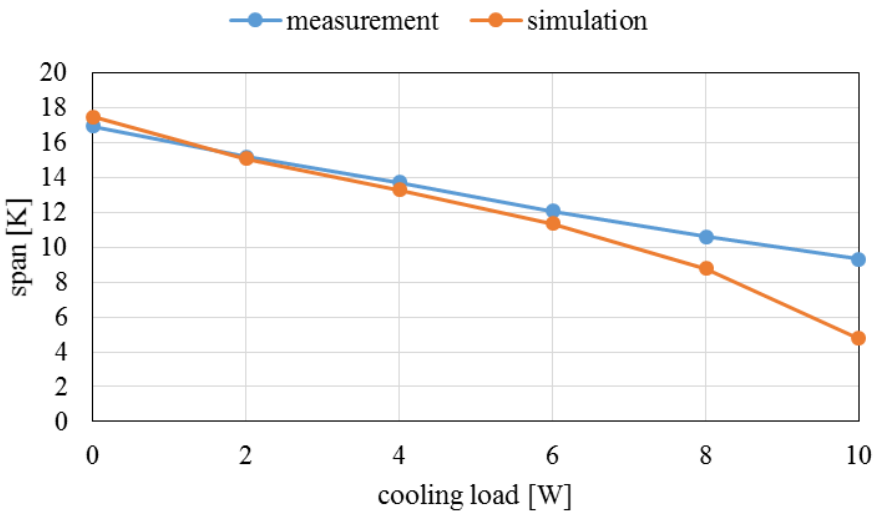

Figure 15: Tests with varied total cooling load with two regenerators filled with gadolinium

The comparison made in this section shows the validity of the simulation results except for very low temperature spans with limited or no practical use.

5 Optimization results for two or 12 regenerators filled with the existing 550 µm, gadolinium spheres or its alloys

The verified model can be used in parametric studies for optimization purposes. In this section the maximum obtainable temperature span in the cases with two and twelve regenerators filled with gadolinium or its alloys are calculated and compared.

With two regenerators filled with gadolinium, the largest obtainable temperature span, with similar test conditions mentioned in section 4 and no cooling load, is simulated to be 20.6 K with cycle frequency of 2.2 Hz and maximum flow rate of 12.5 cm^3s^{-1}. This maximum in temperature span is found through an iterative parametric study in which the maximum flow rate and cycle frequency are varied one at a time. With 4.1 W total cooling load the maximum temperature span is 17.9 K with cycle frequency of 2.8 Hz and maximum flow rate of 18.1 cm^3s^{-1}.

To get more cooling capacity or larger temperature span all the regenerators can be used. For the simulation of the cases with 12 regenerators filled, modeling of the magnetic field and parasitic heat transfer are repeated since they are affected by the change in the number of filled regenerators and added hydraulic connections and hoses. The change in the flow rate and the magnetic field for each regenerator for the case with 12 regenerators filled with gadolinium or gadolinium alloys are shown in Figure 16. With this setup, unlike the case with two regenerators, the magnet cannot be kept stationary to make blow periods longer. Therefore, each regenerator is in high field region only for less than 30° of the continuous rotation of the magnet assembly.

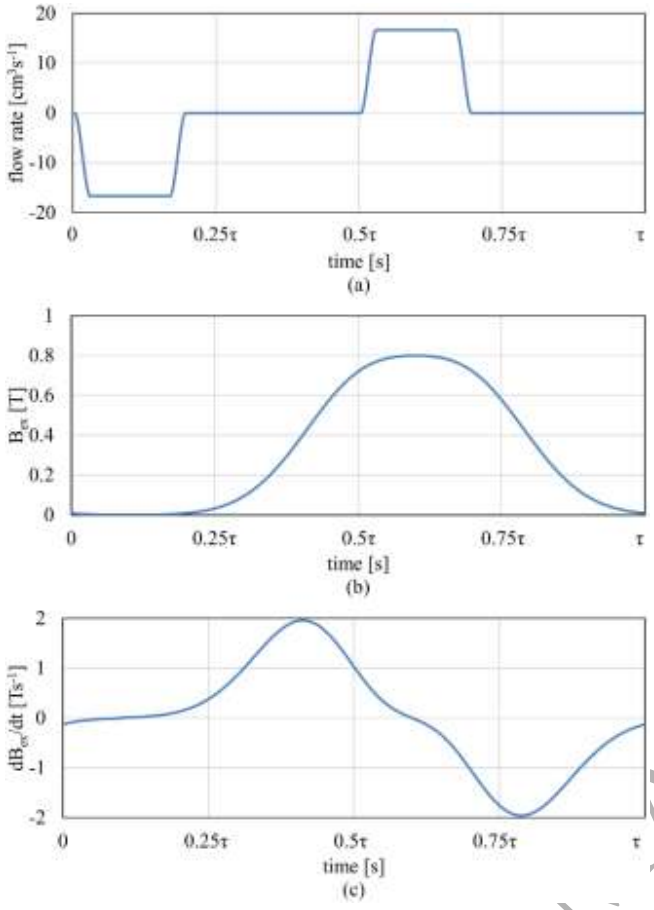

Figure 16: For the case with 12 regenerators filled with Gd or its alloys: (a) flow in each regenerator (the maximum rates can be different in the tests) (b) external field (c) rate of change of the external field

However, with 12 regenerators the cooling capacity will not be six times higher compared to the case with two regenerators mainly because with 12 regenerators the transition between high and low magnetic field is longer relative to the cycle period and the duration of the maximum flow is limited due to the continuous rotation of the magnet assembly and the rotary valve (compare Figure 12 and Figure 16). The prolonged period of transition from low to high magnetic field gives more time to unfavorable phenomena, such as axial conduction from warm end to cold end through the regenerators and outside regenerators and the parasitic heat transfer from the ambient to the regenerators, and thereby reduce the performance. The parasitic heat transfer to the cold end is also higher due to the extra connections and hoses needed, whereas the parasitic heat transfer in azimuthal direction to the neighbor regenerators is lower as they are at similar temperatures during the operation.

With all regenerators filled with 550 µm, spherical particles of gadolinium, not its alloys, the largest obtainable temperature span, with similar test conditions mentioned in section 4 and no cooling load, is found to be 20.5 K with a cycle frequency of 1.6 Hz and a maximum flow rate of

13.9 cm^3s^{-1}. With 4.1 W total cooling load the maximum temperature span is 19.6 K with a cycle frequency of 1.8 Hz and maximum flow rate of 18.1 cm^3s^{-1}.

That the temperature span in the cases with two regenerators and 12 regenerators at no-load condition is not different shows that the limiting factor is the temperature range, within which the magnetocaloric effect is significant, about the Curie temperature of gadolinium. To investigate whether the extra parasitic heat transfer in the case with 12 regenerators is not the reason, optimization is repeated with the assumption that the parasitic heat transfer is the same as that in the case with two regenerators. Under this assumption, the maximum temperature span would be 20.7 K for 0 W cooling loads. That is, for the no-load condition the maximum temperature span is practically the same, however, with 12 regenerators the temperature span with 4.1 W total cooling load is larger compared to the case with two regenerators since the limit imposed by the material properties is not reached yet.

To extend the temperature span further despite the limited useful temperature range about the transition temperature of the materials, layers of gadolinium alloys with different Curie temperatures can be used. It is assumed that these alloys have properties similar to those of gadolinium, without violating the thermodynamic relations between the properties while shifting the Curie temperatures. By choosing the Curie temperatures following the simplified version of the process explained by Monfared and Palm (2015), in which the length of layers are kept equal and their Curie temperatures are varied relative to the average temperature of the layers during the whole cycle, the temperature span of 24.2 K with 30 W total cooling load and 10 layers (the Curie temperature of each is 0.8 K above its average temperature during a cycle) at a cycle frequency of 1.8 Hz and a maximum flow rate of 23.6 cm^3s^{-1} is obtained. The direct comparison with the single-layer case is not possible for 0 W or 4.1 W total cooling loads since the cold end temperature falls below the freezing point of the heat transfer fluid, -6 °C; however, the temperature span obtained with layered beds and with 30 W total cooling load already exceeds that of gadolinium with no cooling load, showing the effectiveness of layering. If the freezing point is ignored, using a hypothetical heat transfer fluid with properties similar to aqueous solution of ethylene glycol (15% by volume) but extended over a wider temperature range to the lowest fluid temperature during the cycle instead of to the freezing point, the temperature span of 32.5 K is estimated for the no-load condition and 10 layers of gadolinium.

In addition to the cycle frequency, flow rate and choice of transition temperature of each layer, for further improving the performance, the size of the particles can also be optimized and the number of layers can be varied. Varying these two parameters is also considered in section 6, where the regenerators are optimized for an application in household or professional refrigerators.

6 Redesigning the regenerators for application in a refrigerator

The original design of the prototype was done for the application in a professional refrigerator, although for ambient temperatures higher than what is considered in this study, a few years ago.

In this work, considering the original purpose of the design, the performance of the prototype with room and refrigerated compartment's temperatures of 22 and 4 °C is simulated with the regenerator layers optimized to maximize the cooling capacity. The temperature difference in both warm and cold heat exchangers are assumed 2 K. This temperature difference, which is smaller than the temperature difference in the heat exchangers of many commercially built refrigerators, implies that rather effective heat exchangers are to be used in the prototype. With the 2 K temperature difference, the return temperatures from the heat exchangers are 24 and 2 °C; that is, an additional benefit of using effective heat exchangers, apart from limiting the temperature span resulting in increased cooling capacity, is that no antifreeze is needed to be blended with water. Without antifreeze, the extra pressure drop due to high viscosity of the heat transfer fluid is avoided. Use of water, the properties of which are assumed unaffected by the anticorrosion agents, for both gadolinium alloys and $La(Fe,Mn,Si)_{13}H_z$ makes also the comparison between them more straightforward.

Unless otherwise stated, the porosity of the beds is 0.36 for the results presented in this section. The obtained results are for moderately insulated cold surfaces. With increasing the insulation (reducing part of the parasitic heat transfer) higher cooling capacities are achievable. In practice, usually the spherical particles provided by the manufacturers are not exactly of the same size; therefore, the expected performance is between or, if the average particle size is close to the optimum value, possibly slightly higher than the predicted performances for the bounds of the range of the particle sizes.

6.1 Results for 12 regenerators filled with gadolinium alloys

For the case with all regenerators filled with gadolinium alloys, the variations of the magnetic field and flow of the heat transfer fluid and parasitic heat transfer are explained in section 5.

Optimization of the parameters to maximize the cooling capacity is done through iterative parametric studies. That is, one parameter is varied at a time and the new optimum found for this parameter is used in other studies in which another parameter varies. This process is repeated until none of the parametric studies suggest a new, better value as the optimum. The final results, showing the variation of one parameter while the rest are at their optimum values, are plotted. The return temperatures from the heat exchangers are 24 and 2 °C in all the simulations presented in this section.

Figure 17 shows how the cooling capacity varies with the change in the particle diameter. The size of the particles affects the heat transfer between the fluid and the solid considerably. The correlation used in this study shows that the solid-fluid heat transfer coefficient, neglecting the heat transfer when the fluid is stationary, is proportional to $d_P^{-0.4}$. The heat transfer coefficient is multiplied by the specific surface area, $a=6(1-\varepsilon)d_P^{-1}$; therefore, the heat transfer rate between solid and fluid for a certain temperature difference is proportional to $d_P^{-1.4}$. Furthermore, the thermal resistance within the solid particle hinders the heat transfer in large particles (see Eq. 11). Accordingly, with too large particles the heat transfer between the solid and fluid is limited,

resulting in reduced cooling capacity. On the other hand, too low particle size increases the pressure drop and viscous dissipation proportional to d_P^{-2} or d_P^{-1} when viscous forces or inertial forces are dominant (Dullien, 1975; Macdonald et al., 1979). Large viscous dissipation has also a negative effect on the cooling capacity.

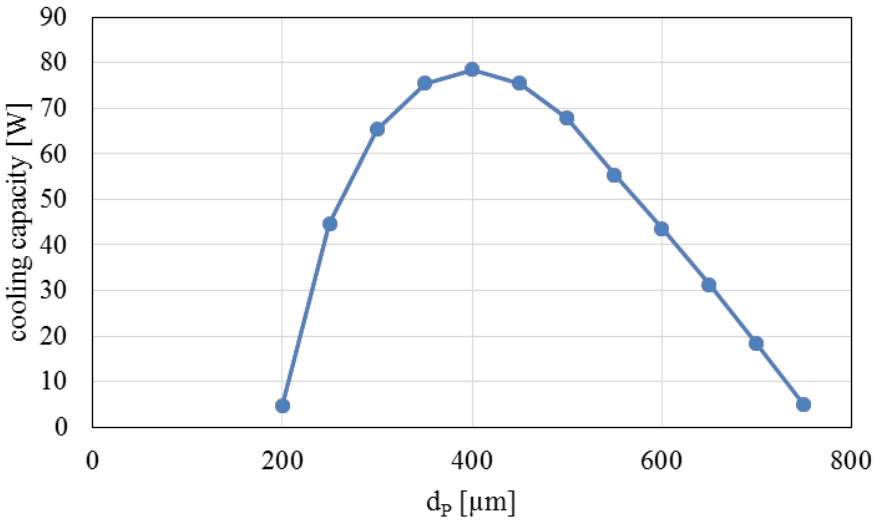

Figure 17: Effect of particle diameter on cooling capacity

As shown in Figure 18, with larger number of layers the cooling capacity can be improved as the transition temperature of the layers match better with their working temperatures. In addition, in practice but not in the simulation results presented here, the large number of layers makes the device less sensitive to small deviations in the Curie temperature of each layer from the calculated ones (Lei et al., 2015). However, when the number of layers is sufficiently large, the further increase does not improve the performance considerably. The reason is that the temperature ranges about the transient temperature of the adjacent layers, in which the magnetocaloric effect is the highest, overlap.

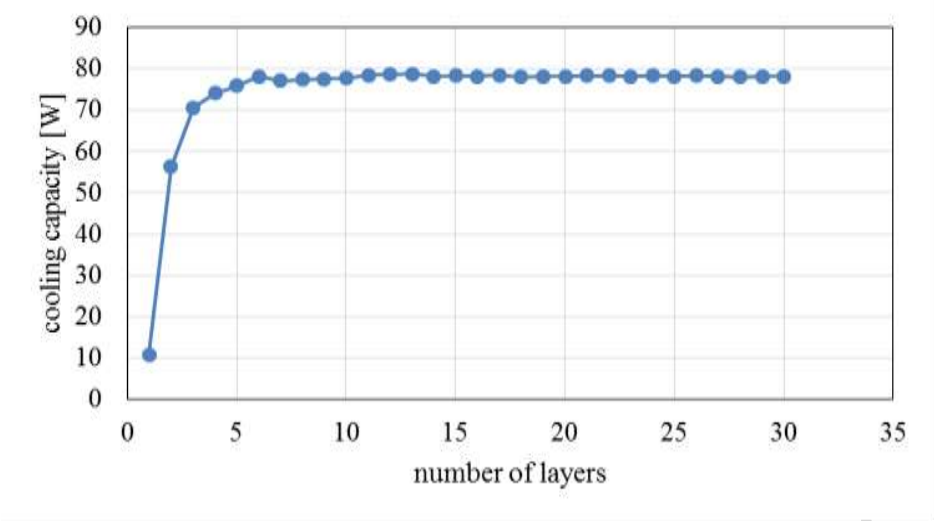

Figure 18: Effect of number of layers on cooling capacity

By increasing the number of completed cycles per unit time more cooling power can be produced. Nevertheless, if the flow rate of the heat transfer fluid is not increased at the same time, the heat generated in the magnetocaloric materials cannot be carried away or the heat from the cold heat exchanger cannot be delivered to the demagnetized materials at the same rate and the increase in frequency becomes ineffective (see Figure 19 and Figure 20). Higher flow rate means more effective heat transfer through both advection and solid-fluid convection heat transfer, which results in higher cooling capacities. However, the benefit of increasing the flow rate too much is limited by the excessive pressure drop that it causes; therefore, there is a decline in the cooling capacity after the peak in Figure 20.

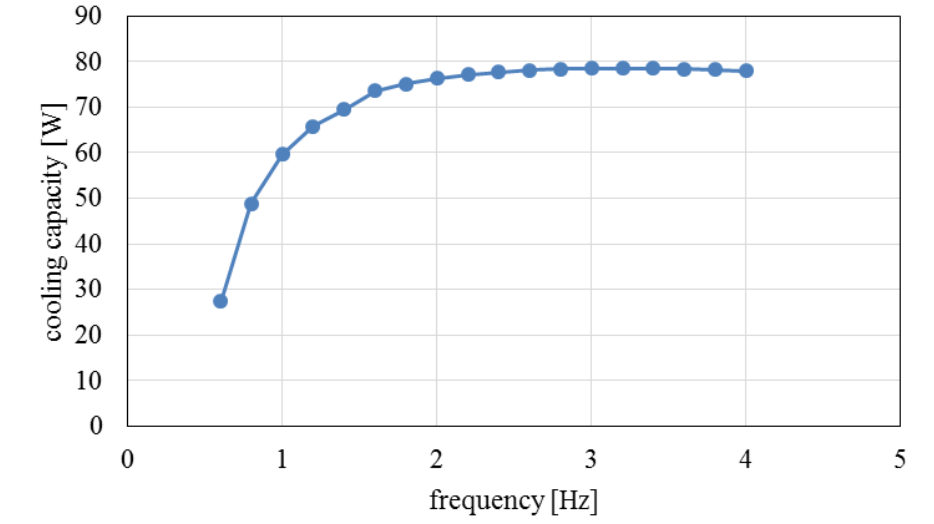

Figure 19: Effect varying the cycle frequency on cooling capacity

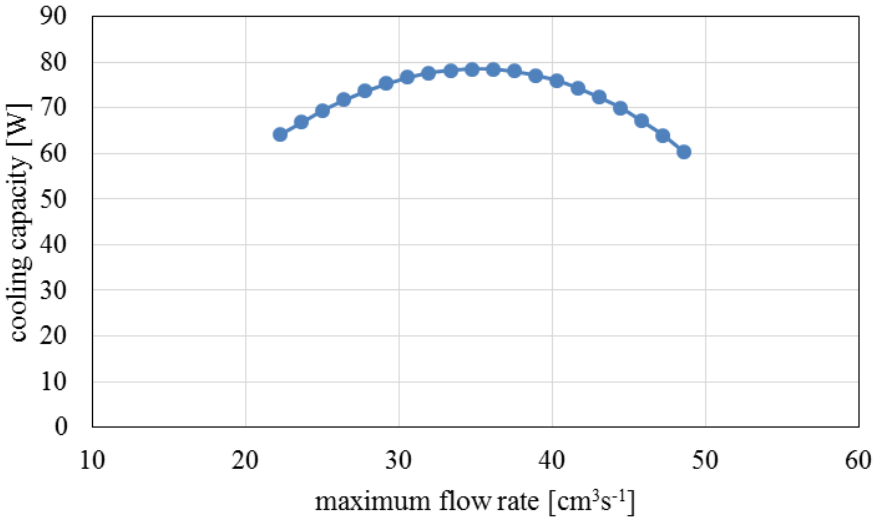

Figure 20: Effect of maximum flow rate on cooling capacity

Figure 21 shows how the Curie temperatures of each layer are optimally chosen to maximize the cooling capacity. The variable on the horizontal axis is the difference between the Curie temperature of a layer and the average temperature of the magnetocaloric material in that layer during a cycle. In line with the results published by Monfared and Palm (2015) better performance is achieved when the Curie temperature of a layer is above the average temperature of that layer during a cycle. The optimal value of this difference is determined by the shape of the magnetocaloric effect diagrams and the cycle.

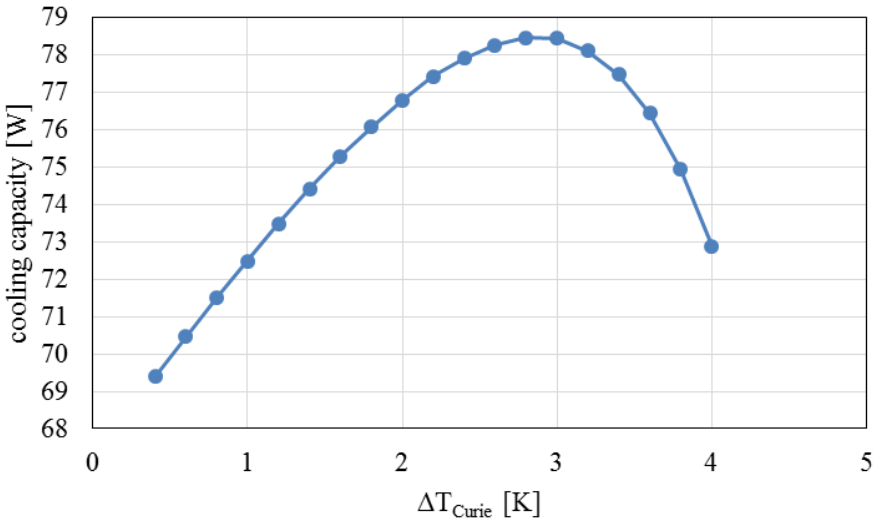

Figure 21: Effect of choosing Curie temperature for each layer on cooling capacity

In a side study in which porosity is also optimized together with the other parameters a maximum cooling capacity of 90 W is calculated; however, in practice the porosity cannot be varied or controlled easily while making packed beds.

6.2 Results for 12 regenerators filled with $La(Fe,Mn,Si)_{13}H_z$

With $La(Fe,Mn,Si)_{13}H_z$ instead of gadolinium alloys, the model of the parasitic heat transfer and variation in flow rate remain unchanged. The variation in the field, however, is modeled again since it is affected by the magnetic properties of the materials by which the regenerators are filled. The same iterative procedure for optimization as described in section 6.1 is used for the regenerators filled with $La(Fe,Mn,Si)_{13}H_z$ and the final results are presented for both epoxy bonded and non-bonded particles in Figure 22. These are the results from the final iteration, which means that in each plot the parameters, except the ones on the horizontal axes and number of layers, are the optimum ones giving the highest cooling capacity.

Unlike the regenerators with gadolinium alloys, as Figure 22b suggests, the number of layers needed to get a high cooling capacity with $La(Fe,Mn,Si)_{13}H_z$ is large. It is expected owing to the fact that in materials with first-order phase transition the peak in magnetocaloric effect is narrower. However, similar to the case with gadolinium alloys, increasing the number of layers after getting close to the maximum capacity does not improve the capacity considerably. In the simulations presented in Figure 22, apart from Figure 22b, 22 layers are used.

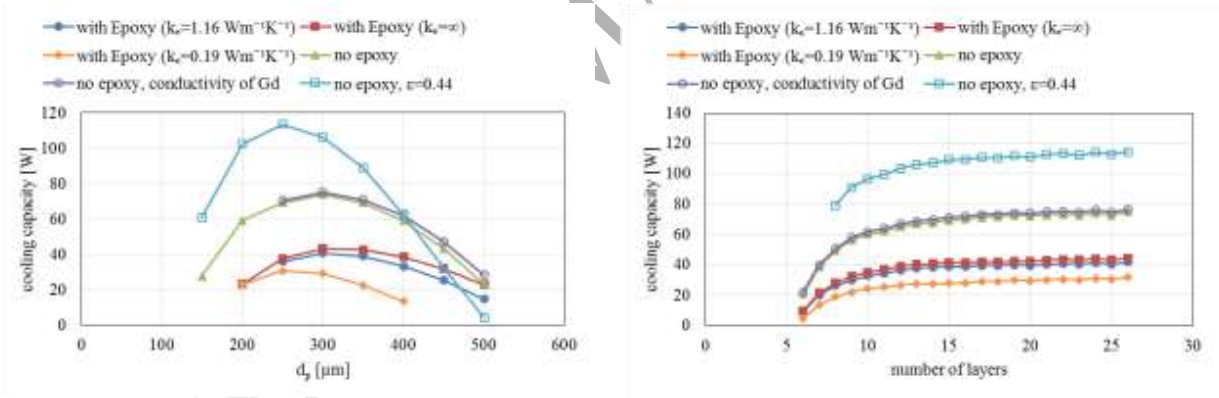

(a) (b)

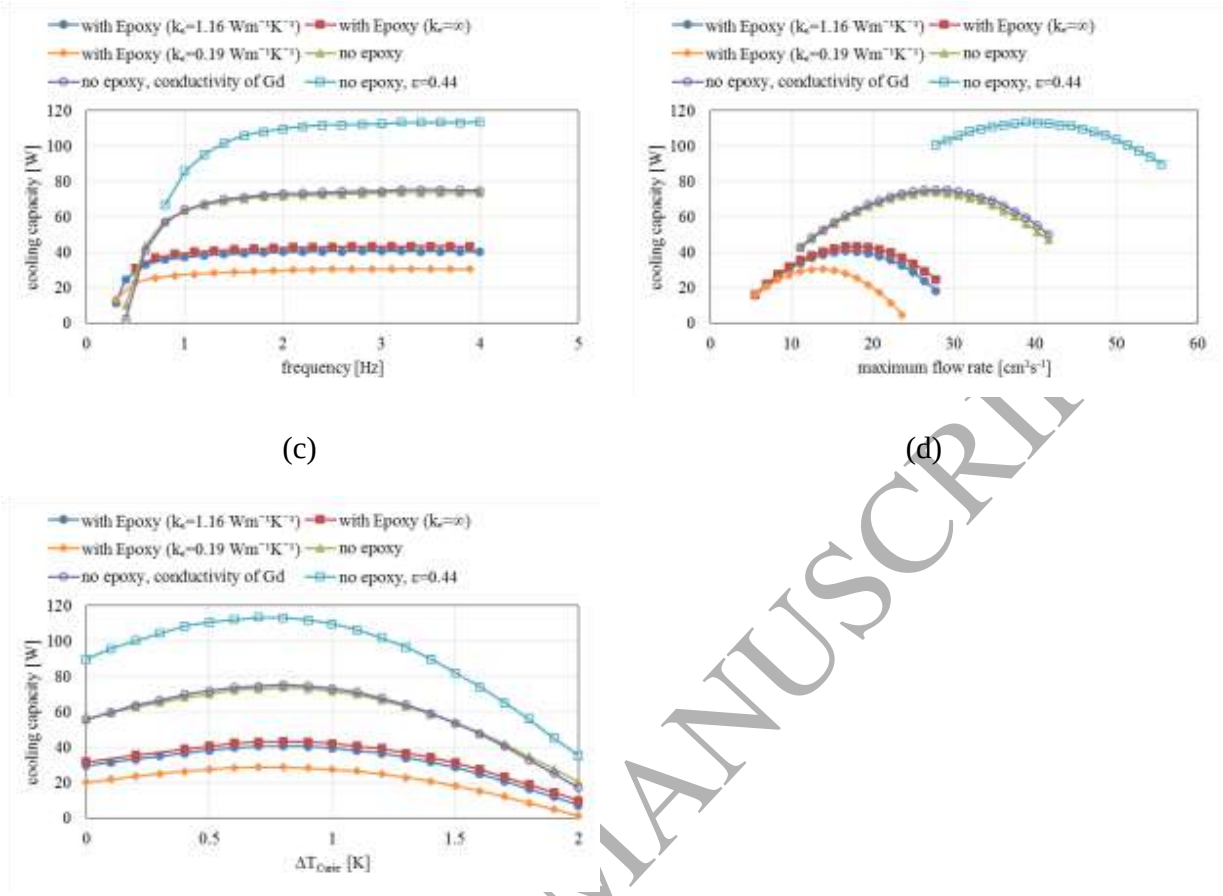

Figure 22: Optimization results for 12 regenerators filled with $La(Fe,Mn,Si)_{13}H_z$, with and without epoxy as binding agent

Comparing the results of epoxy bonded and non-bonded regenerators shows that the layer of epoxy with the given properties reduces the cooling capacity considerably. With the moderate thermal conductivity of 1.16 $Wm^{-1}K^{-1}$, the layer of epoxy reduces the cooling capacity mainly through increasing the pressure drop due to its relatively low density and also, to a lesser extent, evident from the curves where the thermal resistance of epoxy is neglected, through increasing the thermal resistance between the particles and the heat transfer fluid. However, if the thermal conductivity of epoxy is low, 0.19 $Wm^{-1}K^{-1}$ here, it acts as an insulating layer over the refrigerant particles and decreases the performance even further. Since the regenerators' casing was originally designed for much larger temperature spans they are thin and long, which makes them sensitive to pressure drop. In this work redesigning the regenerators are done for the existing prototype; therefore, optimizing cross section area and length of the regenerators is beyond the scope of this study.

Even without epoxy and with the porosity of 0.36, the value used also for the simulations with gadolinium alloys, the expected enhancement in cooling capacity through using $La(Fe,Mn,Si)_{13}H_z$ is not observed. The lower thermal conductivity of $La(Fe,Mn,Si)_{13}H_z$ is not the limiting factor here since the repeated optimization process with thermal conductivity of $La(Fe,Mn,Si)_{13}H_z$ replaced by that of gadolinium resulted in slightly improved results, as presented in Figure 22. In fact, the pressure drop is the limiting factor. In an earlier experiment with irregularly shaped $La(Fe,Mn,Si)_{13}H_z$ particles the mass of the magnetocaloric materials put into the regenerators were measured accurately and the porosity of the beds were calculated to be 0.44 using the density (Russek et al. (2010) have also reported a rather high porosity value, 0.47, for similar irregular particles). With the higher porosity, which lowers the pressure drop, smaller particles and higher flow rates can be used resulting in more effective heat transfer in the regenerators and, therefore, higher cooling capacities compared to gadolinium, as shown in Figure 22. However, it is not certain whether the higher porosity is actually due to the empty spaces left between the irregular particles or it is merely an error caused by the assumption of a constant density for all of the layers in spite of their different composition. Since the porosity of the packed beds cannot be easily controlled in practice, optimizing its value may not have direct practical use; however, to investigate the potential of $La(Fe,Mn,Si)_{13}H_z$ as compared to gadolinium, a side study with porosity optimized together with the previously mentioned parameters is done. With optimized porosity, over 200 W cooling capacity is calculated for regenerators filled with $La(Fe,Mn,Si)_{13}H_z$, while the maximum cooling capacity with gadolinium for the same working temperatures is 90 W.

It should be noted that the Ergun equation or its modified version (Macdonald et al., 1979) has been used to predict the pressure drop in the bonded beds, just as was done by other investigators (Burdyny and Rowe, 2013; Jacobs et al., 2014; Wysokinski et al., 2002). However, the applicability of this equation to bonded beds has, to the best knowledge of the author, not been confirmed.

7 Conclusions

To simulate the performance of a magnetic refrigeration prototype, it is modeled in three parts: modeling the magnetic field and its variations; modeling the parasitic heat transfer; modeling the active magnetic regeneration cycle. In modeling the magnetic field, which is validated against measured magnetic field, it is shown that neglecting the presence of the magnetocaloric materials and their influence on the magnetic field can result in inaccurate modeling of the applied magnetic field and thereby the internal field sensed by the magnetocaloric materials. The model of the magnetic field is three dimensional; however, it is argued that a spatial average value can be used in the model of the active magnetic regeneration cycle. The model of parasitic heat transfer is also three dimensional and detailed; nevertheless, with an innovative method it is implemented in the one dimensional model of the active magnetic regeneration cycle without

compromising the accuracy. As shown in the validation process the results of the simulation program are very close to the experimental ones.

The verified simulation model of the prototype is used to optimize the regenerators to maximize the cooling capacity. The necessity of layering and using materials showing first order phase transition are also investigated.

Although some of the materials with first-order phase transition, such as $La(Fe,Mn,Si)_{13}H_z$, are potentially more effective refrigerants than are the materials with second-order phase transition, it should be noted that in designs with high pressure drop, such as the investigated regenerators in this study, their potential may not be fully exploited. The reason is that to carry away the extra heating or cooling created by those materials during magnetization and demagnetization higher heat transfer rates are needed which result in possibly too high viscous dissipation counterbalancing the extra cooling potential of the refrigerant. Another disadvantage of the packed bed design for $La(Fe,Mn,Si)_{13}H_z$ is the need for a bonding agent, which, depending on the properties of the used agent, can add to the pressure drop and resistance to heat transfer between the particles and the heat transfer fluid.

With the long and narrow regenerators of the prototype, for which the simulations are run, the higher potential of the investigated material with first order phase transition, $La(Fe,Mn,Si)_{13}H_z$, cannot be exploited due to the high pressure drop in the packed beds. It is shown that the low thermal conductivity of $La(Fe,Mn,Si)_{13}H_z$ (compared to gadolinium) is not the limiting factor here. Further investigations reveal that increasing the void space between the particles can decrease the viscous dissipation so much that it overcompensates for the reduced amount of refrigerant and can increase the cooling capacity significantly. Nevertheless, controlling the void fraction in packed beds may not be feasible in practice.

For epoxy bonded beds, the effect of epoxy on heat transfer rates are corrected using the derived correlations. If thermal conductivity of epoxy is low, 0.19 $Wm^{-1}K^{-1}$ in this study, this extra thermal resistance, together with the added pressure drop, lowers the performance. In case the epoxy has a moderate thermal conductivity, 1.16 $Wm^{-1}K^{-1}$ in this study, the largest negative effect of epoxy is on pressure drop by narrowing the flow passages in the regenerators of the prototype. However, investigating the accuracy of adopting the equations giving the pressure drop in non-bonded packed beds to bonded beds is of interest as further studies. If epoxy with low thermal conductivity (0.19 $Wm^{-1}K^{-1}$ investigated in this study) is used, the performance is significantly affected by the epoxy layer acting as insulation over the magnetocaloric particles.

8 Acknowledgements

I would gratefully like to acknowledge that this study was financed by the Swedish Energy Agency, grant number 40330-1, and Electrolux through the research program EFFSYS EXPAND.

I would also like to thank Prof. Björn Palm for his suggestions and sharing time and the Department of Energy Conversion and Storage, Technical University of Denmark, specifically Christian Bahl, Kurt Engelbrecht, and Kristina Navickaité, for providing us gadolinium particles and their measured properties.

The computations were performed on resources provided by the Swedish National Infrastructure for Computing (SNIC) at PDC Centre for High Performance Computing (PDC-HPC).

9 References

Amiri, A., & Vafai, K. (1998). Transient analysis of incompressible flow through a packed bed. *International Journal of Heat and Mass Transfer, 41*(24), 4259-4279. doi:10.1016/S0017-9310(98)00120-3

Arnold, D. S., Tura, A., Ruebsaat-Trott, A., & Rowe, A. (2014). Design improvements of a permanent magnet active magnetic refrigerator. *International Journal of Refrigeration, 37*(0), 99-105. doi:10.1016/j.ijrefrig.2013.09.024

Bahl, C. R. H., Navickaitė, K., Neves Bez, H., Lei, T., Engelbrecht, K., Bjørk, R., . . . Shen, B. (2017). Operational test of bonded magnetocaloric plates. *International Journal of Refrigeration, 76*, 245-251. doi:10.1016/j.ijrefrig.2017.02.016

Balli, M., Jandl, S., Fournier, P., & Kedous-Lebouc, A. (2017). Advanced materials for magnetic cooling: Fundamentals and practical aspects. *Applied Physics Reviews, 4*(2), 021305. doi:10.1063/1.4983612

Balli, M., Sari, O., Mahmed, C., Besson, C., Bonhote, P., Duc, D., & Forchelet, J. (2012). A pre-industrial magnetic cooling system for room temperature application. *Applied Energy, 98*(Supplement C), 556-561. doi:10.1016/j.apenergy.2012.04.034

Bjørk, R., & Bahl, C. R. H. (2013). Demagnetization factor for a powder of randomly packed spherical particles. *Applied Physics Letters, 103*(10). doi:10.1063/1.4820141

Bjørk, R., Bahl, C. R. H., Smith, A., & Pryds, N. (2010). Review and comparison of magnet designs for magnetic refrigeration. *International Journal of Refrigeration, 33*(3), 437-448. doi:10.1016/j.ijrefrig.2009.12.012

Bleaney, B., & Hull, R. A. (1941). The Effective Susceptibility of a Paramagnetic Powder. *Proceedings of the Royal Society of London. Series A. Mathematical and Physical Sciences, 178*(972), 86.

Burdyny, T., & Rowe, A. (2013). Simplified modeling of active magnetic regenerators. *International Journal of Refrigeration, 36*(3), 932-940. doi:10.1016/j.ijrefrig.2012.10.022

Dixon, A. G., & Cresswell, D. L. (1979). Theoretical prediction of effective heat transfer parameters in packed beds. *AIChE Journal, 25*(4), 663-676. doi:10.1002/aic.690250413

Dullien, F. A. L. (1975). Single phase flow through porous media and pore structure. *The Chemical Engineering Journal, 10*(1), 1-34. doi:10.1016/0300-9467(75)88013-0

Engelbrecht, K. (2008). *A Numerical Model of an Active Magnetic Regenerator Refrigerator with Experimental Validation.* (PhD), University of Wisconsin-Madison,

Engelbrecht, K., Eriksen, D., Bahl, C. R. H., Bjørk, R., Geyti, J., Lozano, J. A., . . . Pryds, N. (2012). Experimental results for a novel rotary active magnetic regenerator. *International Journal of Refrigeration, 35*(6), 1498-1505. doi:10.1016/j.ijrefrig.2012.05.003

Fujieda, S., Hasegawa, Y., Fujita, A., & Fukamichi, K. (2004). Thermal transport properties of magnetic refrigerants La(FexSi1−x)13 and their hydrides, and Gd5Si2Ge2 and MnAs. *Journal of Applied Physics, 95*(5), 2429-2431. doi:10.1063/1.1643774

Fukamichi, K., Fujita, A., & Fujieda, S. (2006). Large Magnetocaloric Effects and Thermal Transport Properties of La(FeSi)13 and Their Hydrides. *ChemInform, 37*(19), no-no. doi:10.1002/chin.200619005

Jacobs, S., Auringer, J., Boeder, A., Chell, J., Komorowski, L., Leonard, J., . . . Zimm, C. (2014). The performance of a large-scale rotary magnetic refrigerator. *International Journal of Refrigeration, 37*(0), 84-91. doi:10.1016/j.ijrefrig.2013.09.025

Kitanovski, A., Tušek, J., Tomc, U., Plaznik, U., Ožbolt, M., & Poredoš, A. (2015). *Magnetocaloric Energy Conversion: From Theory to Applications*: Springer.

Lei, T., Nielsen, K. K., Engelbrecht, K., Bahl, C. R. H., Neves Bez, H., & Veje, C. T. (2015). Sensitivity study of multi-layer active magnetic regenerators using first order magnetocaloric material La(Fe,Mn,Si)13Hy. *Journal of Applied Physics, 118*(1), 014903. doi:10.1063/1.4923356

Lozano, J. A., Capovilla, M. S., Trevizoli, P. V., Engelbrecht, K., Bahl, C. R. H., & Barbosa, J. R. (2016). Development of a novel rotary magnetic refrigerator. *International Journal of Refrigeration, 68*, 187-197. doi:10.1016/j.ijrefrig.2016.04.005

Lozano, J. A., Engelbrecht, K., Bahl, C. R. H., Nielsen, K. K., Barbosa Jr, J. R., Prata, A. T., & Pryds, N. (2014). Experimental and numerical results of a high frequency rotating active magnetic refrigerator. *International Journal of Refrigeration, 37*(0), 92-98. doi:10.1016/j.ijrefrig.2013.09.002

Macdonald, I. F., El-Sayed, M. S., Mow, K., & Dullien, F. A. L. (1979). Flow through Porous Media-the Ergun Equation Revisited. *Industrial & Engineering Chemistry Fundamentals, 18*(3), 199-208. doi:10.1021/i160071a001

Melinder, Å. (2010). *Properties of Secondary Working Fluids for Indirect Systems* (2nd ed.). France: IIF-IIR.

Monfared, B., & Palm, B. (2015). Optimization of layered regenerator of a magnetic refrigeration device. *International Journal of Refrigeration, 57*, 103-111. doi:10.1016/j.ijrefrig.2015.04.019

Monfared, B., & Palm, B. (2016). *New magnetic refrigeration prototype with application in household and professional refrigerators*. Paper presented at the 7th International Conference on Magnetic Refrigeration at Room Temperature, Thermag VII, Turin.

Morrish, A. H. (2001). *The physical principles of magnetism*. New York: IEEE Press.

Morrison, K., Sandeman, K. G., Cohen, L. F., Sasso, C. P., Basso, V., Barcza, A., . . . Gutfleisch, O. (2012). Evaluation of the reliability of the measurement of key magnetocaloric properties: A round robin study of La(Fe,Si,Mn)Hδ conducted by the SSEEC consortium of European laboratories. *International Journal of Refrigeration, 35*(6), 1528-1536. doi:10.1016/j.ijrefrig.2012.04.001

Neves Bez, H., Navickaité, K., Lei, T., Engelbrecht, K., Barcza, A., & Bahl, C. (2016). *Epoxy-bonded La(Fe,mn,si)13Hz As A Multi Layered Active Magnetic Regenerator*. Paper presented at the the 7th International Conference on Magnetic Refrigeration at Room Temperature, Turin. 10.18462/iir.thermag.2016.0147

Nield, D. A., & Bejan, A. (2013). *Convection in Porous Media*. New York, NY: Springer New York :.

Nielsen, K. K., Nellis, G. F., & Klein, S. A. (2013). Numerical modeling of the impact of regenerator housing on the determination of Nusselt numbers. *International Journal of Heat and Mass Transfer, 65*, 552-560. doi:10.1016/j.ijheatmasstransfer.2013.06.032

Okamura, T., Rachi, R., Hirano, N., & Nagaya, S. (2007). *Improvement of 100w Class Room Temperature Magnetic Refrigerator*. Paper presented at the 2nd IIF-IIR International Conference on Magnetic Refrigeration at Room Temperature, Portoroz, Slovenia.

Pecharsky, V. K., & Gschneidner Jr, K. A. (1999). Magnetocaloric effect and magnetic refrigeration. *Journal of Magnetism and Magnetic Materials, 200*(1–3), 44-56. doi:10.1016/s0304-8853(99)00397-2

Radulov, I. A., Skokov, K. P., Karpenkov, D. Y., Gottschall, T., & Gutfleisch, O. (2015). On the preparation of La(Fe,Mn,Si)13Hx polymer-composites with optimized magnetocaloric properties. *Journal of Magnetism and Magnetic Materials, 396*, 228-236. doi:10.1016/j.jmmm.2015.08.044

Romero Gómez, J., Ferreiro Garcia, R., De Miguel Catoira, A., & Romero Gómez, M. (2013). Magnetocaloric effect: A review of the thermodynamic cycles in magnetic refrigeration. *Renewable and Sustainable Energy Reviews, 17*, 74-82. doi:10.1016/j.rser.2012.09.027

Russek, S., Auringer, J., Boeder, A., Chell, J., Jacobs, S., & Zimm, C. (2010). *The performance of a rotary magnet magnetic refrigerator with layered beds*. Paper presented at the Fourth IIF-IIR International Conference on Magnetic Refrigeration at Room Temperature, Baotou, China.

Sari, O., & Balli, M. (2014). From conventional to magnetic refrigerator technology. *International Journal of Refrigeration, 37*(Supplement C), 8-15. doi:10.1016/j.ijrefrig.2013.09.027

Tura, A., & Rowe, A. (2011). Permanent magnet magnetic refrigerator design and experimental characterization. *International Journal of Refrigeration, 34*(3), 628-639. doi:10.1016/j.ijrefrig.2010.12.009

Wakao, N., & Kaguei, S. (1982). *Heat and Mass Transfer in Packed Beds*. New York: Gordon and Breach, Science Publishers, Inc.

Wysokinski, T. W., Xu, X., & Barclay, J. A. (2002). Monolithic versus conventional packed bed second stage regenerator evaluation in a Gifford–McMahon cryocooler. *Cryogenics, 42*(11), 691-696. doi:10.1016/S0011-2275(02)00137-6